JOURNAL OF MATERIALS SCIENCE **40** (2005) 6079–6086

Secondary electromagnetic radiation during plastic deformation and crack propagation in uncoated and tin coated plain-carbon steel

B. SRILAKSHMI*, A. MISRA
Department of Mechanical Engineering, Birla Institute of Technology, Mesra-835215, Ranchi, India
E-mail: bsl81@rediffmail.com

Published online: 8 September 2005

This paper presents some new results on the emission of electromagnetic radiation (EMR) during plastic deformation, crack initiation and propagation, and fracture of uncoated and tin–coated 0.15% carbon steel sheets. Intermittent EMR emissions have been observed even at stationary loading, which we term as secondary EMR emissions. These results are expected to provide an insight into the micro-mechanism of dislocation relaxation dynamics in metallic materials.

1. Introduction

Observations of the emission of Electromagnetic Radiation (EMR) during plastic deformation and fracture in metals and alloys, and generation of a high transient magnetic field during necking in cylindrical plain-carbon steel specimens, including a bio-physical approach in head injuries, have earlier been reported in a series of papers by one of the authors, Misra [1–14]. The EMR has recordable amplitude varying from a few mV to 1 V depending upon the design of antenna, and has a wide range of frequency spectrum of kHz to 10^{14} Hz. Misra [6] reported a limiting frequency in MHz region and Molotskii [15] proposed a dislocation mechanism for this new effect and based on the dynamics of an edge dislocation in a viscous medium, calculated a limiting frequency in MHz region. Tudik and Valuev [16] reported EMR emission during fracture of iron and aluminium, of rather large frequency. Using photomultiplier, they were able to detect EMR at wavelengths from ∼300 nm to >1500 nm for iron and its alloys and from ∼650 nm to >1500 nm for aluminium and its alloys. Dickinson, Jenson, and Bhattacharya [17] reported the emission of EMR during crack propagation and fracture at the interface of aluminium and epoxy. Jagashivamani and Iyer [18] confirmed and explored this new effect further. Using semi-cylindrical copper antenna they detected EMR in kHz range.

Now with the discovery of new smart materials/composites, this EMR effect becomes important in the sense that this EMR can itself be utilized in developing smart sensors, coated/embedded into a material matrix. The problem is to identify an element which gives rise to maximum EMR response under minimum mechanical stimulus. This element can then be incorporated into the main material through a suitable surface engineering technique and thus set a new trend in the development of smart material/composites. With this aim in view, experiments were conducted to investigate the effect of coating on EMR emission and the results are being reported here.

2. Experimental

2.1. Materials and specimens

Experiments were conducted on 0.3 mm thick 0.15% carbon steel sheets with standard tin coating compositions, E-25 (with equal coating of 5.6 gm/m^2 of tin), E-75 (with equal coating of 16.8 gm/m^2 of tin), and D-11.2/5.6 (with differential coating of 11.2/5.6 gm/m^2 of tin). These sheets were obtained from Tin-plate company, and were manufactured by applying tin-coating on both sides of the steel sheets through an electrolytic tin coating process at speeds upto 11 m/s. Experiments were also conducted on uncoated 0.15% carbon steel sheets for comparison of results.

Now, the fracture of flawed components may be analyzed by a stress analysis based on concepts of elastic theory. Using modifications of analytical methods, solutions for crack-tip stress distributions associated with the three major modes of fracture loading, viz. opening, shearing, and tearing have been presented by various researchers [19]. These modes involve different crack surface displacements. In mode I or opening mode, crack surfaces move directly apart, whereas in mode II, sliding or in-plane shearing, crack surfaces slide over one another in a direction perpendicular to the leading edge of the crack. In mode III, tearing or

*Author to whom all correspondence should be addressed.
0022-2461
DOI: 10.1007/s10853-005-1293-4

antiplane shear mode, crack surfaces move relative to one another and parallel to the leading edge of the crack [19]. It may be noted that mode I fracture loading is encountered in the overwhelming majority of actual engineering situations involving cracked components. Mode II is found less frequently and is of little engineering importance. Mode III may be regarded as a pure shear problem such as that involving a notched round bar in torsion. Therefore, it was decided to investigate the effect of tin-coating on the emission of EMR under opening (mode I) and tearing (mode III) modes of fracture loadings.

For the opening and tearing mode tests all specimens had overall dimensions of 100 mm × 14 mm × (0.3 + coating thickness) mm, cut with the longitudinal axis along the rolling direction of the sheet. An initial single straight edge notch (notch length $a = 7$ mm, corresponding to the standard notch-depth ratio $a/w = 0.5$) was provided by a fine jeweller scissor, while for the tearing mode test, a central longitudinal cut of 85 mm was provided in the specimens as shown in Fig. 1.

Effect of notch-depth ratio (a/w) on the EMR emission in opening mode was also investigated with E-25 and D-11.2/5.6 specimens cut along both parallel and perpendicular to the rolling directions of the sheets. Single edge straight initial notch of lengths $a = 3, 5, 7, 9$ and 11 mm, were provided in the specimens.

Specimens cut with their longitudinal axis along the rolling direction of the sheet have been designated as E-25, E-75, and D-11.2/5.6 respectively, while specimens cut with their longitudinal axis along perpendicular to the rolling directions have been designated as PE-25, PE-75, and PD-11.2/5.6 respectively.

2.2. Instrumentation

For mechanical loading, a manually operated one-tonne capacity horizontal Hounsfield tensometer was employed. A newly designed antenna was adopted for detecting the EMR signals this time, which could detect some new results, missed in the earlier experiments. For this, 10 mm × 5 mm × 0.1 mm copper foil chips joined electrically were fixed by adhesives with proper insulation on the two opposite surfaces of each specimen, as shown in Fig. 1. This copper chips-combination acted as an antenna for the EMR signals. A 150 MHz Analog-digital HAMEG oscilloscope model HM1507-3 with built- in software SP107 FFT (Beta version) was used for capturing the signals. This software had Fast Fourier Transformation (FFT) facility to convert time domain EMR signals into frequency domain. An IBM Pentium IV personal computer was used for data storage and processing. An RS232 interface was used for transferring the data from oscilloscope to computer. Trigger level was kept just above the noise level of the laboratory to avoid interference of noise with signal, and a time scale of 10 μs/div was maintained on the oscilloscope, which could capture signals upto MHz range.

Since the EMR amplitude and frequency recorded, depend upon the design of the antenna and also upon its distance from the crack propagation zone, experiments

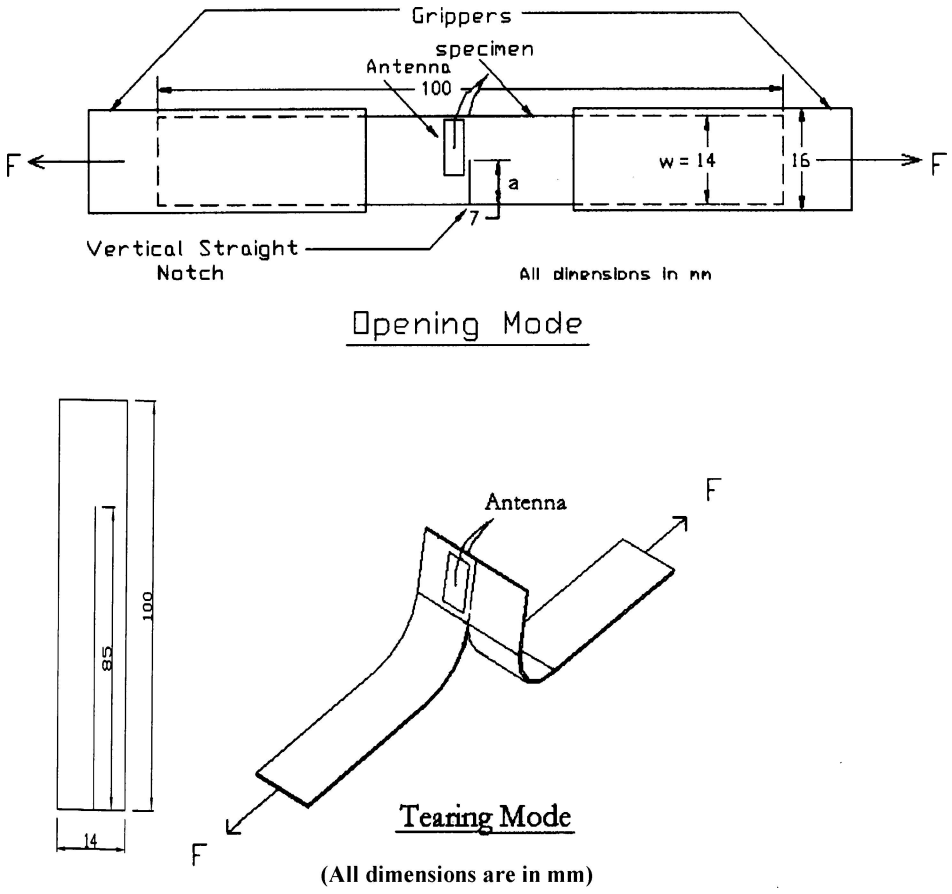

Figure 1 Specimens in opening and tearing modes of fracture with antenna positioning.

were conducted with various antenna distances. It was observed that with increase in antenna distance, (i) total number of EMR signals recorded, decreased, (ii) maximum EMR amplitude did not show much difference for the distances (1 to 4 mm) tested, (iii) frequency components in kHz range did not show much difference, but (iv) *MHz component signals were missed*. Hence on the basis of some trial experiments an antenna distance of 1 mm from the initial notch/slit was maintained in all the experiments.

3. Results and discussions

3.1. Modes of fracture

Fig. 1 shows the specimen configurations and antenna position in opening and tearing modes of fracture. Intermittent EMR signals of varying amplitudes were emitted from the specimens in both opening and tearing modes of fracture, *prior to crack initiation*, during crack propagation and fracture.

In almost all specimens, an interesting phenomenon was observed in both opening and tearing modes of fracture: since oscilloscope had to be tuned to 'single-shot mode' for capturing these transient EMR signals, every time after the oscilloscope captured one transient signal, it switched off. Further mechanical loading of the specimen had to be stopped and the oscilloscope had again to be tuned to 'single-shot mode' for future EMR signal. It was observed that the specimens emitted additional EMR signals even 'without further mechanical loading'. We term these EMR emissions as 'Secondary Emission' for clarity of presentation. These secondary emissions were observed several times during the entire mechanical loading till fracture in both tin-coated and uncoated steel specimens under both opening and tearing modes of fracture. These signals were missed during the earlier research because an *U*-shaped antenna was employed for the detection of EMR signals, which could not detect these signals due to a large gap between the antenna and the crack propagation region. Here we have termed Primary Emissions as those EMR signals which are emitted with increasing mechanical loading.

Fig. 2a and b are the printouts of one such primary and secondary emissions (upper graphs) emitted during the opening mode of fracture of PE-25 specimen, with their FFT superimposed (lower graphs); (primary emission: maximum amplitude, $V_{\text{pmax}} = 5$ mV, maximum dominant frequency, $f = 49.42$ kHz, 1.08 MHz; secondary emission: maximum amplitude, $V_{\text{pmax}} = 4$ mV, maximum dominant frequency, $f = 57.33$ kHz, 1.10 MHz). In several cases, secondary emissions were observed even more than six to eight times after an intermittent primary emission. Further, in almost all specimens tested, EMR signals of frequencies varying from few kHz to few MHz range were recorded. The FFT recorded distinct low EMR amplitude with MHz component frequencies varying between 1 and 14 MHz. Since the specimen after emitting a primary emission was still under mechanical load though stationary, with the position of the loading wheel held constant, it is possible that the accelerated dislocation/crack relaxation gives rise to the observed secondary EMR emissions.

Another point may be noteworthy here: during the electrolytic process of tin coating, hydrogen may enter the material as a result of cathodic charging and undermine fracture resistance by simultaneously introducing another cracking process. Troiano [20] has argued that hydrogen diffuses under the influence of a stress gradient regions of high tensile triaxiality which then interacts with the metal lattice to lower its cohesive strength. A decrease in the cohesive energy of the grain boundary lowers the local stress necessary to generate an accelerating micro-crack [19]. Therefore, it is possible that hydrogen entrapment during the cathodic charging coating process may cause formation of micro- cracks during the stationary loading and these micro-cracks are responsible for the emission of secondary EMR. However, this proposed mechanism requires further experimental verification.

When the tin-coated specimen surface was examined intermittently during the test and after final fracture, mesh/branch-type crack formation was observed in the tin-coated specimen surfaces spread over a region of about 8 mm on both sides of the propagating crack. This was not remarkably visible in uncoated steel specimens. This coating layer crack-mesh/branch generation appears to be responsible for larger number of EMR emissions. Fig. 2c shows a sample photograph of the crack mesh/branch appearance on the surface of the fractured specimens.

Now, during stressing, all grains/dislocations undergoing cracking/oscillations, generate EMR signals but due to the inherent skin-depth characteristics, EMR signals generated within the core region of the material are incapable of escaping out. i.e, they are screened off. Therefore, what is being observed is basically the EMR signals emitted from the grains/dislocations present within the outer surface skin depth layer of the material. The skin-depth for most of the materials is of the order of 1.0 μm whereas the tin-coating in E-25 specimens is 0.7644 μm thick and in E-75 specimens it is 2.2992 μm. Therefore, it is possible that some EMR signals in E-75 specimens are screened off giving the pattern: steel $<$ E-75 $<$ E-25, for total number (primary plus secondary) of emissions in both opening and tearing modes of fracture.

Figs 3 and 4 are the bar charts for V_{pmax}, number of primary emissions (N_{p}) and number of secondary emissions (n) for uncoated and tin-coated 0.15% carbon steel sheets (E-25, E-75, and D-11.2/5.6) fractured under opening and tearing modes respectively. Fig. 5a and b show the bar chart of the dominant EMR frequency (kHz and MHz ranges) in these materials under the opening and tearing modes of fracture. An inspection of these figures shows the correlations presented in Table I.

Since the antenna chips were attached on both sides of the specimens and electrically joined together, it was not possible to isolate the contributions to EMR of 11.2 gm/m^2 tin-coating on one surface and 5.6 gm/m^2 tin-coating on the other surface. For this reason, the D-11.2/5.6 data have been compared separately in Table I.

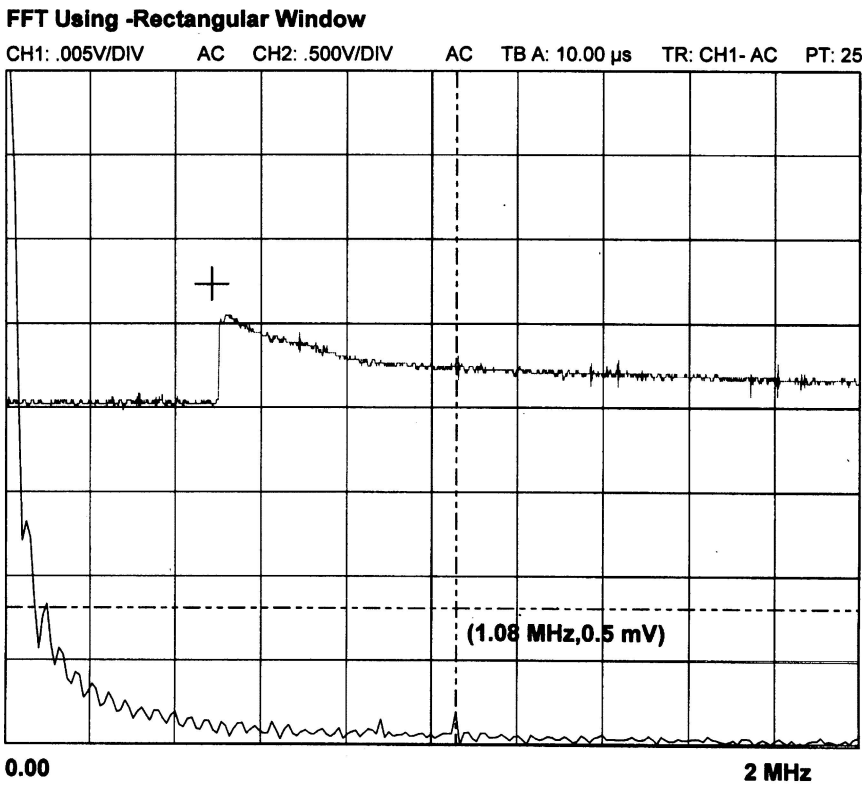

(a)

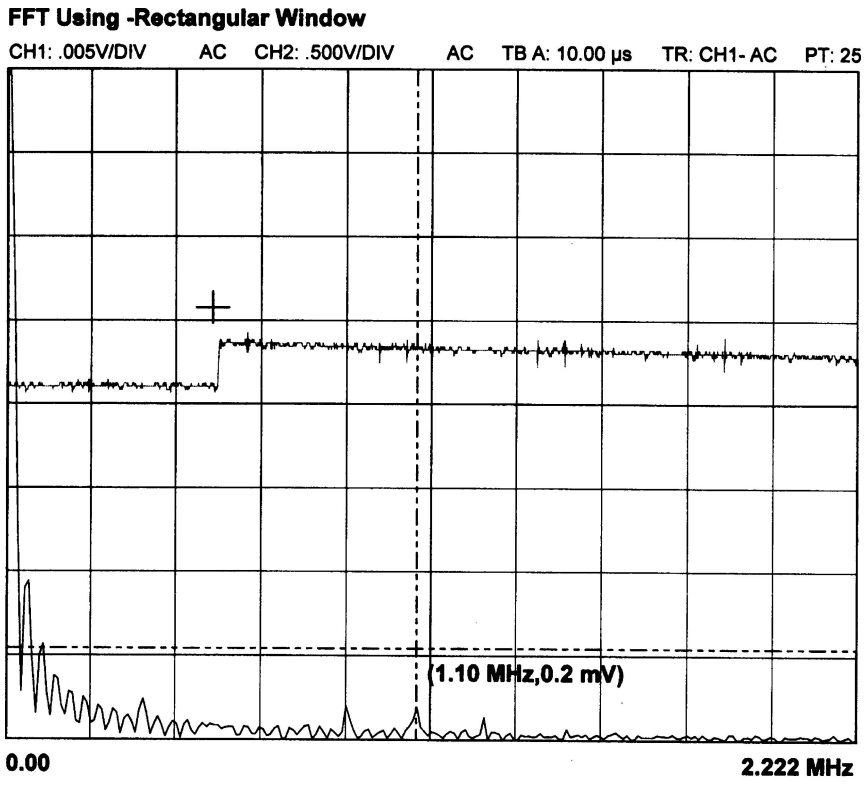

(b)

Figure 2 (a) One sample primary EMR emission with FFT in the opening mode of fracture in PE-25 tin-coated steel. (b) One sample secondary EMR emission with FFT in the opening mode of fracture in PE-25 tin-coated steel, corresponding to the primary emission shown in Fig. 2a. (c) Photograph of mesh/branch type surface crack formation near the fracture edge of the E-25 specimen under tearing mode. (magnification 20×). (*Continued on next page*).

From Table I, it is clear that

(1) $V_{\text{pmax}} \propto 1/f_{\text{max}}$ in both the modes of fracture. It may be noted here that V_{pmax} and f_{max} do not correspond to the same EMR signal. From among the several EMR signals emitted during stressing of each specimen, maximum EMR amplitude is V_{pmax} and maximum frequency is f_{max}.

(2) Primary emissions (N_{p}) are largest in the differentially coated specimens under both opening and tearing

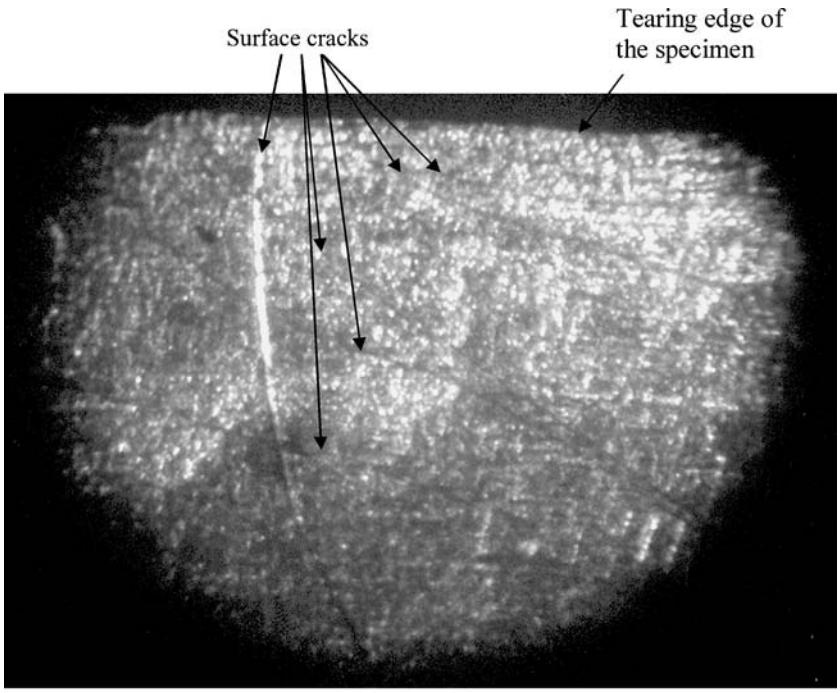

(c)

Figure 2 Continued.

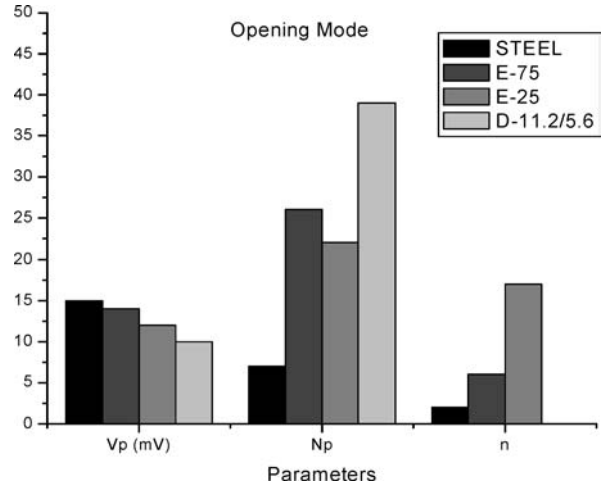

Figure 3 Maximum EMR peak amplitude (V_{pmax}) number of primary emission (N_P) and secondary emission (n) in materials under opening mode of fracture.

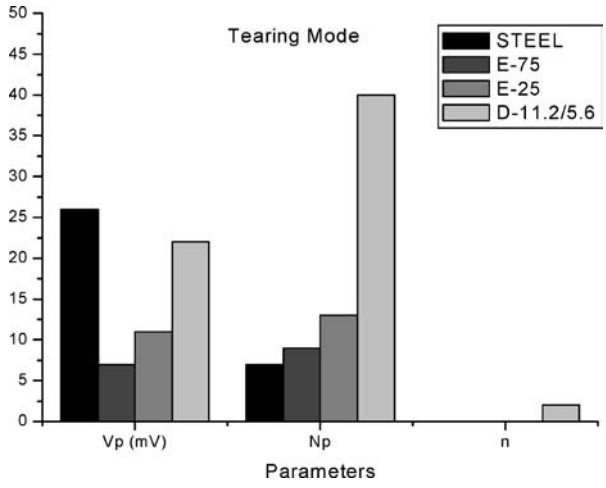

Figure 4 Maximum EMR peak amplitude (V_{pmax}) number of primary emission (N_P) and secondary emission (n) in materials under tearing mode of fracture.

modes of fracture. Further, primary emissions are larger in all tin-coated specimens as compared to uncoated specimens. Earlier research works, for example [13] show that the EMR emission during crack propagation in tin is less than that in steel. However, tin in steel is known to cause severe metallurgical embrittlement

TABLE I Comparison of EMR parameters in uncoated and tin- coated steel sheets

Mode	Parameter	Uncoated vs. equally coated sheets	Uncoated vs. differentially coated sheets
Opening	V_{pmax}	Steel > E-75 > E-25	Steel > D-11.2/5.6
	f_{max} (kHz)	Steel < E-75 < E-25	Steel < D-11.2/5.6
	f_{max} (MHz)	Steel < E-75 < E-25	Steel < D-11.2/5.6
	N_P	Steel < E-25 < E-75	Steel < D-11.2/5.6
	n	Steel < E-75 < E-25	No secondary emission in D-11.2/5.6
Tearing	V_{pmax}	Steel > E-25 > E-75	Steel > D-11.2/5.6
	f_{max} (kHz)	Steel < E-25 < E-75	Steel < D-11.2/5.6
	f_{max} (MHz)	Steel < E-25 < E-75	Steel < D-11.2/5.6
	N_P	Steel < E-75 < E-25	Steel < D-11.2/5.6
	n	No secondary emission	Secondary emission in D-11.2/5.6 only

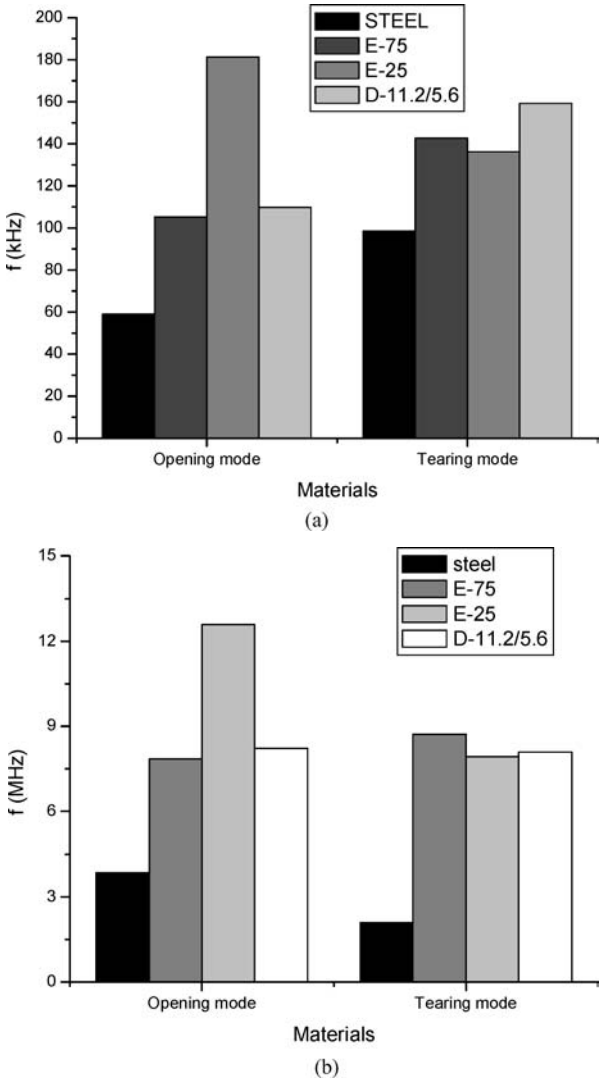

Figure 5 (a) Maximum EMR frequency in kHz range (f_{max}) in materials under opening and tearing modes of fracture. (b) Maximum EMR frequency in MHz range (f_{max}) in materials under opening and tearing modes of fracture.

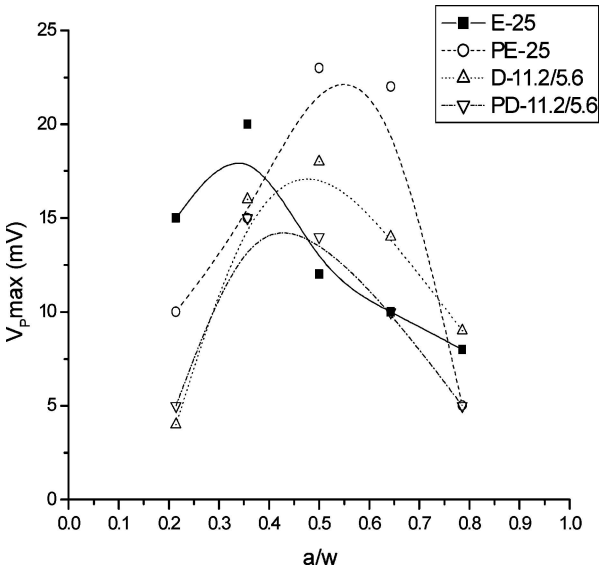

Figure 6 Variation of maximum EMR peak amplitude ($V_p$max) with notch-depth ratio (a/w) in materials.

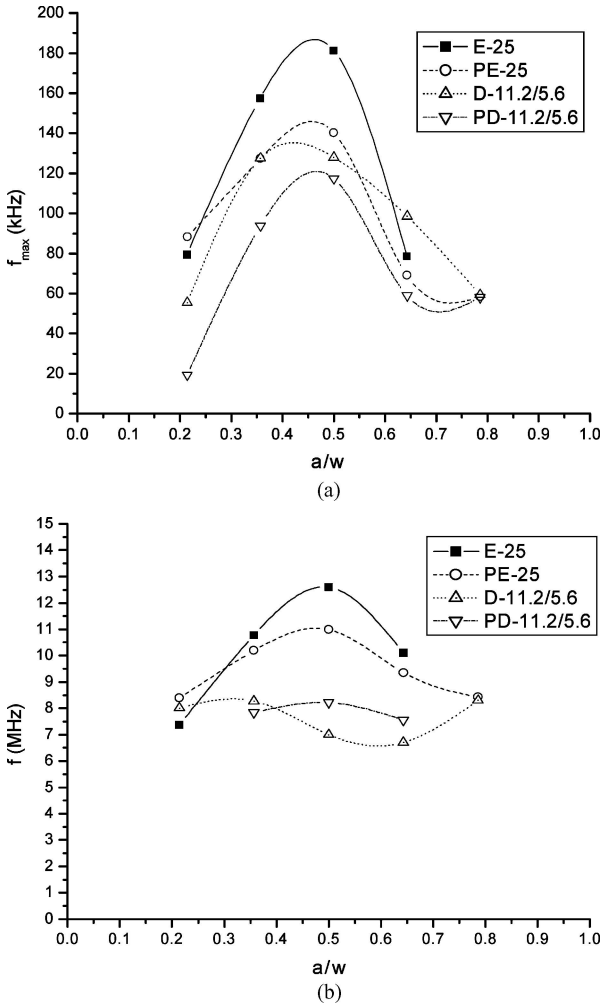

Figure 7 Variation of dominant kHz component frequency (f_{max}) with notch-depth ratio (a/w) in materials.

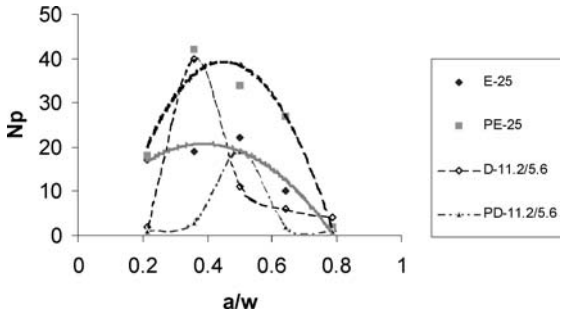

Figure 8 Variation of number of primary EMR emissions (N_p) with notch-depth ratio (a/w) in materials.

[19]. Moreover, cathodic charging coating introduces the possibility of further cracking process due to hydrogen entrapment at the tin-steel interface. Therefore, tin–coated steel specimens emit larger number of primary and secondary EMR emissions than the uncoated steel specimens.

(3) However, differentially coated specimens did not show any secondary emission in opening mode of fracture (but it gave secondary emissions when these specimens were fractured under opening mode *with their longitudinal axis perpendicular to the rolling direction of the sheet*—to be discussed later.)

(4) Under tearing mode of fracture, only differentially coated specimens showed secondary emissions.

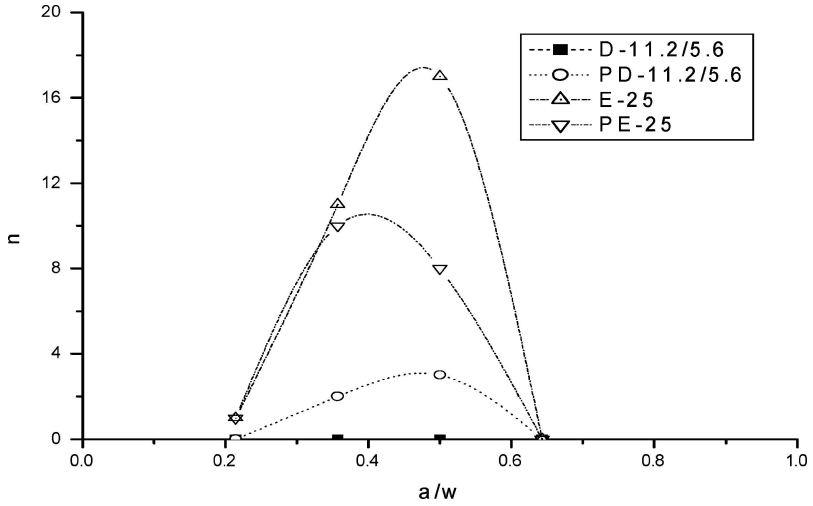

Figure 9 Variation of number of secondary EMR emissions (n) with notch-depth ratio (a/w) in materials.

3.2. Effect of notch-depth ratio and rolling directions

Figs 6–9 show the variations of V_{pmax}, f_{max}, N_{P}, and n with notch-depth ratio (a/w) for the four types of specimens, E-25, PE-25, D-11.2/5.6, and PD-11.2/5.6, as designated earlier. It may be noted here that the applied force F in Fig. 1, under the opening mode, induces an additional bending component also. This results in a net compressive stress in the outer portion of the remainder (w-a) section of the specimen. A simple elasticity analysis shows that this compressive zone is maximum at $a/w = 0.5$ [21]. The accelerated dislocations emanating from the crack tip, therefore, suffers maximum hindrance to its motion due to this compressive zone at $a/w = 0.5$ and results in enhanced EMR emission. It is probably due to this fact that all the curves of Figs 6–9 except one curve in Fig. 7b show maxima at around $a/w = 0.5$.

Let θ be the angle between the longitudinal axis of the specimen (hence the direction of force F) and the rolling direction of the steel sheet matrix. Then specimens of category E-25 and D-11.2/5.6 have $\theta = 0^\circ$, while category PE-25 and PD-11.2/5.6 have $\theta = 90^\circ$. V_{pmax} curves of E-25 and PE-25 show maxima at $a/w = 0.34$ and $a/w = 0.56$ respectively (Fig. 6), thus showing a dependency of V_{pmax} on θ. Since intensity of radiation is proportional to the square of the amplitude, it appears that higher intensity radiation components are emitted from the steel portions of the specimens because the tensile strength of steel sheet depends upon θ. However, the maxima of V_{pmax} curves in D-11.2/5.6 and PD-11.2/5.6 specimens appear to be only slightly dependent on θ. This shows that as overall thickness of coating layer is increased (thickness of D-11.2/5.6 > E-25) the emission from tin-coating layer dominates due to the screen effect, and the dependency of maxima of V_{P} on θ decreases.

The fact that the maximum frequency is independent of θ except the MHz component in differentially coated specimens (Fig. 7a and b), shows that higher frequency components of EMR observed, are emitted from the surface layers of tin-coating only.

In contrast to V_{pmax} curves, primary emissions (N_{P}) show a clear dependency on θ in differentially coated specimens (Fig. 8). Now, when the surfaces of the specimens were examined, criss-cross mesh crack patterns were observed to be different on the two surfaces of the specimens of D-11.2/5.6 and PD-11.2/5.6 categories. It is well known that the tensile strength of steel varies along the different rolling directions, giving rise to difference in stress level on the surface layers. Therefore, the stress distributions in the tin-coating in D-11.2/5.6 and PD-11.2/5.6 specimens become different, giving rise to difference in crack branching. Hence it appears that two different maxima in Fig. 8 for the primary EMR emissions are obtained because of different crack branching in the two coating layers on the surfaces.

Finally, Fig. 9 shows an interesting pattern for the secondary emissions. The D-11.2/5.6 specimens did not emit any secondary emission, while the rest three show almost similar pattern. None of the specimens emitted secondary emissions for $a/w < 0.214$ and $a/w > 0.643$. E-25 and PD-11.2/5.6 specimens show maximum secondary emissions at $a/w = 0.5$ where as PE-25 show maxima at $a/w \sim 0.4$.

4. Conclusions

On the basis of the above experimental results, following conclusions can be drawn:

- Metals emit secondary EMR. This may be due to accelerated cracks/dislocations relaxation. This observation will help in understanding the micro-mechanism of dislocation relaxation dynamics within the metallic materials.
- The maximum amplitude of EMR is inversely proportional to the maximum frequency.
- Surface coating crack formation emits EMR in general, independent of the rolling direction and hence independent of the micro-structural characteristics of the matrix metal.

Further research in this direction is in progress and will be reported in due course.

Acknowledgement

Research grant from the Department of Science and Technology, Government of India, is gratefully acknowledged.

References

1. A. MISRA, *Ind. J. Pure Appl. Phys.* **11** (1973) 419.
2. *Idem.*, *Nature (London)* **254** (1975) 133.
3. *Idem.*, "Ninth Yearbook to the Encyclopedia of Science and Technology" (Edizioni Scientifiche E Tecniche, Mondadori, Italy, 1975).
4. *Idem.*, in "Discovery of Stress-Induced Magnetic and Electromagnetic Effects in Metals" (D.Sc. Dissertation, Ranchi University, 1976).
5. *Idem.*, *Phys. Lett.* **62A** (1977) 234.
6. *Idem.*, *Appl. Phys.* **16** (1978) 195.
7. *Idem.*, *J. Scient. Ind. Res.* **40** (1981) 22.
8. A. MISRA and S. GHOSH, *Ind. J. Pure Appl. Phys.* **18** (1980) 851.
9. *Idem.*, *Appl. Phys.* **23** (1981) 387.
10. A. MISRA, *Neurol. Ind.* **XXVIII** (1980) 234.
11. A. MISRA and B. G. VARSHNEY, *J. Magn. Magn. Mater.* **89** (1990) 159.
12. B. SRILAKSHMI and A. MISRA, in International Conference on Advances in Surface Treatment: Research and Applications. (Hyderabad, India, 2003).
13. A. MISRA and A. KUMAR, *Intern. J. Fract.* **127** (2004) 387.
14. *Idem.*, *J. Magn. Magn. Mater.* **285** (2005) 71.
15. M. I. MOLOTSKII, *Sov. Techn Phys. Lett.* **6** (1980) 22.
16. A. A. TUDIK and N. P. VALUEV, *Sov Techn. Phys. Lett.* **6** (1980) 37.
17. J. T. DICKINSON, L. C. JENSON and S. K. BHATTACHARYA, *J. Vac. Sci. Technol.* **3** (1985) 1398.
18. V. JAGASIVAMANI and K. J. IYER, *Mater. Lett* **6** (1988) 418.
19. R. W. HERTZBERG, in "Deformation and Fracture Mechanics of Engineering Materials" 4th edn. (John Wiley and Sons, Inc., 1996) pp. 462, 494.
20. A. R. TROIANO, *Trans. ASM* **52** (1960) 54.
21. B. SRILAKSHMI and A. MISRA, *Manuf Techn. Res.—An Intern. J.* (in press)

Received 27 September 2004
and accepted 31 March 2005